

University of Louisville

ThinkIR: The University of Louisville's Institutional Repository

Faculty Scholarship

10-1-2020

The Sizes of $z \sim 9-10$ Galaxies Identified in the Brightest of Reionizing Galaxies (BoRG) Survey

Benne W. Holwerda

University of Louisville, benne.holwerda@louisville.edu

Joanna S. Bridge

University of Louisville

Rebecca L. Steele

University of Louisville

Samir Kusmic

University of Louisville

Larry Bradley

STScI

See next page for additional authors

Follow this and additional works at: <https://ir.library.louisville.edu/faculty>



Part of the [Astrophysics and Astronomy Commons](#)

ThinkIR Citation

Holwerda, Benne W.; Bridge, Joanna S.; Steele, Rebecca L.; Kusmic, Samir; Bradley, Larry; Livermore, Rachael; Bernard, Stephanie; and Jacques, Alice, "The Sizes of $z \sim 9-10$ Galaxies Identified in the Brightest of Reionizing Galaxies (BoRG) Survey" (2020). *Faculty Scholarship*. 473.

<https://ir.library.louisville.edu/faculty/473>








This Article is brought to you for free and open access by ThinkIR: The University of Louisville's Institutional Repository. It has been accepted for inclusion in Faculty Scholarship by an authorized administrator of ThinkIR: The University of Louisville's Institutional Repository. For more information, please contact thinkir@louisville.edu.

Authors

Benne W. Holwerda, Joanna S. Bridge, Rebecca L. Steele, Samir Kusmic, Larry Bradley, Rachael Livermore, Stephanie Bernard, and Alice Jacques



The Sizes of $z \sim 9$ – 10 Galaxies Identified in the Brightest of Reionizing Galaxies (BoRG) Survey

Benne W. Holwerda¹ , Joanna S. Bridge¹ , Rebecca L. Steele¹ , Samir Kusmic¹ , Larry Bradley² , Rachael Livermore^{3,5} ,
Stephanie Bernard⁴ , and Alice Jacques¹

¹ Department of Physics and Astronomy, 102 Natural Science Building, University of Louisville, Louisville KY 40292, USA; benne.holwerda@louisville.edu

² Space Telescope Science Institute, 3700 San Martin Drive, Baltimore 20218 MD, USA

³ School of Physics, The University of Melbourne, Parkville, VIC, 3010, Australia

⁴ School of Physics, University of Melbourne & ARC Centre of Excellence for All-Sky Astrophysics (CAASTRO), Australia

Received 2018 October 5; revised 2020 May 6; accepted 2020 May 6; published 2020 September 4

Abstract

Redshift $z = 9$ – 10 object selection is the effective limit of Hubble Space Telescope (HST) imaging capability, even when confirmed with Spitzer. If only a few photometry data points are available, it becomes attractive to add criteria based on their morphology in these J - and H -band images. One could do so through visual inspection, a size criterion, or alternate morphometrics. We explore a vetted sample of Brightest of Reionizing Galaxies (BoRG) $z \sim 9$ and $z \sim 10$ candidate galaxies and the object rejected by Morishita+ to explore the utility of a size criterion in $z = 9$ – 10 candidate selection. A stringent, point-spread function (PSF)-corrected effective radius criterion ($r_e < 0''.3$) would result in the rejection of 65%–70% of the interlopers visually rejected by Morishita et al. It may also remove up to $\sim 20\%$ of bona fide brightest ($L \gg L^*$) $z = 9$ or 10 candidates from a BoRG selected sample based on the Mason et al. luminosity functions, assuming the Holwerda et al. $z \sim 9$ size–luminosity relation. We argue that including a size constraint in lieu of a visual inspection may serve in wide-field searches for these objects in, e.g., Euclid or HST archival imaging with the understanding that some brightest ($L \gg L^*$) candidates may be missed. The sizes of the candidates found by Morishita et al. follow the expected size distribution of $z \sim 9$ for bright galaxies, consistent with the log normal in Shibuya et al. and single objects. Two candidates show high star formation surface density ($\Sigma_{\text{SFR}} > 25 M_{\odot} \text{ kpc}^{-2}$) and all merit further investigation and follow-up observations.

Unified Astronomy Thesaurus concepts: [High-redshift galaxies \(734\)](#); [Galaxies \(573\)](#); [Lyman-break galaxies \(979\)](#); [Galactic and extragalactic astronomy \(563\)](#); [Galaxy classification systems \(582\)](#); [Galaxy distances \(590\)](#); [Galaxy evolution \(594\)](#); [Galaxy radii \(617\)](#); [Galaxy stellar content \(621\)](#); [Galaxy formation \(595\)](#)

1. Introduction

Near-infrared deep observations with the Hubble and Spitzer Space Telescopes as well as ground-based surveys have resulted in a boon in the numbers of high-redshift galaxies ($z > 6$) identified by the Lyman-break in their optical and near-infrared colors. The high-redshift frontier is now firmly at $z \sim 9$ – 10 , the limit of Hubble Space Telescope (HST) Lyman dropout technique, with a dozen high-fidelity candidates known (Bouwens et al. 2011a, 2011b, 2013; Zheng et al. 2012; Coe et al. 2013; Ellis et al. 2013; Oesch et al. 2013, 2014). These highest redshift candidates can be identified by their extremely red near-infrared colors ($J - H > 0.5$), a lack of flux in bluer (optical) bands, and—when available—relatively blue H – $4.5 \mu\text{m}$ colors. The fainter $z \sim 9$ – 10 candidates were found both behind lensing clusters (Zheng et al. 2012; Coe et al. 2013), and in ultra-deep e Wide Field Camera 3 (WFC3)/infrared observations (Bouwens et al. 2011b; Ellis et al. 2013; Oesch et al. 2013).

The brightest objects at these redshifts are exceedingly rare but a number of them have been identified in both the Cosmic Assembly Near-infrared Deep Extragalactic Legacy Survey (CANDELS) deep fields (Oesch et al. 2014) and more recently in HST pure-parallel observations (Calvi et al. 2016; Morishita et al. 2018). The existence of bright ($>L^*$) galaxies poses a critical challenge for early galaxy evolution during the first 500 Myr ($10 - 30\times$ growth from $z \sim 10$ to $z \sim 7$; Madau & Dickinson 2014; Bouwens et al. 2015; Ishigaki et al. 2018), as

these few objects are too bright for the observed evolution of the luminosity function (LF), hinting at a different formation mechanism of the brightest galaxies.

Their relative luminosity and spatial paucity should make these ideal targets for deep near-infrared imaging surveys conducted from the ground (e.g., UltraVISTA; McCracken et al. 2012). However, their reliable detection and selection has proved challenging: 20% of the luminous $z \sim 7$ candidate objects were rejected as spurious with HST follow-up (Bowler et al. 2015) and Stefanon et al. (2017) could not reliably confirm any $z > 8$ candidates using HST follow-up. Therefore, as the widest tier of the near-infrared imaging searches for $z > 7$ bright sources, the Brightest of Reionizing Galaxies (BoRG) survey stands the best chance to identify candidate $z \sim 9$ – 10 galaxies.

There are three mostly independent tests for the high-redshift nature of $z \sim 9$ – 10 galaxy candidates: (a) one can obtain the Spitzer flux and color of these candidates to confirm their photometric redshift (Roberts-Borsani et al. 2016; Bridge et al. 2019), (b) one can observe the Ly α emission line if a (re)ionized bubble is present (Oesch et al. 2015; Zitrin et al. 2015; Stark et al. 2017; Larson et al. 2018), and (c) comparing these sizes against expectations for luminous galaxy candidates at $z \sim 9$ – 10 and the sizes of potential interlopers (Grazian et al. 2012; Holwerda et al. 2015).

The analytical models from Fall & Efstathiou (1980) and Mo et al. (1998) predict that effective radii should scale with redshift somewhere between $\propto(1+z)^{-1}$ for galaxies living in halos of fixed mass or $\propto(1+z)^{-1.5}$ at a fixed circular velocity. Observational evidence from earlier samples also points to such

⁵ ARC DECRA Fellow.

scaling relations, with some studies preferring $(1+z)^{-1}$ (Bouwens et al. 2004, 2006; Oesch et al. 2010), some studies preferring $(1+z)^{-1.5}$ (Ferguson et al. 2004), and some studies lying somewhere in between (Hathi et al. 2008; Ono et al. 2013; Shibuya et al. 2015). For the bright ($>0.3L^*$) sources, one expects galaxies to follow the $\propto(1+z)^{-1.5}$ relation (see Holwerda et al. 2015).

In this paper, we examine the sizes of a sample of $z \sim 9$ –10 candidate galaxies identified in Morishita et al. (2018). Our aim is to evaluate how well candidate galaxy size can be used in the pre-selection of sources without relying on visual assessment. For near-future larger area searches, the addition of an additional criterion other than color will be invaluable. This paper is organized as follows. Section 2 describes the data and catalog used, Section 3 explores the relation between HST colors and effective radii for selected and rejected candidate $z \sim 9$ –10 galaxies, Section 4 shows the redshift evolution of the effective radii, Section 5 compares the inferred star formation surface densities to previously identified bright sources, and Section 6 briefly lists our concluding remarks. We assume a flat cosmology of $H_0 = 73 \text{ km s}^{-1} \text{ Mpc}^{-1}$, $\Omega_0 = 0.28$. For L^* luminosity, we use the $z = 3$ value: $M_{1600}(z = 3) = 21.07$ (Steidel et al. 1999). We provide a Jupyter notebook and the underlying data files that can be used to create the plots in this article on Zenodo under a Creative Commons Attribution license, doi:10.5281/zenodo.3945569.

2. BoRG[z9] Survey Data

Legacy field investigations with HST have covered substantial area ($>800 \text{ arcmin}^2$; Grogin et al. 2011; Koekemoer et al. 2011), and the latest $z > 7$ samples are approaching $\sim 1 \text{ k}$ sources (e.g., Bouwens et al. 2015; Finkelstein et al. 2015). However, at the bright end of the galaxy luminosities, the rarity of high-redshift candidate galaxies is problematic with their cosmic variance being the main source of uncertainty (Barone-Nugent et al. 2014). A few large, contiguous fields can be significantly affected by cosmic variance (Trenti & Stiavelli 2008).

The BoRG survey (Trenti et al. 2011, 2012; Bradley et al. 2012; Schmidt et al. 2014; Calvi et al. 2016) has been designed specifically to contribute toward an unbiased measurement of the number density of the brightest galaxies at $z \sim 8$ initially and now focuses on $z \sim 9$ –10, using HST pure-parallel opportunities to cover a comparable area with medium-deep optical and infrared imaging but with effectively random pointings (5σ , $m_{AB} < 26.5$) over ~ 140 independent sight lines so far.

The initial BoRG survey aimed at the bright end of the LF at $z \sim 8$, using four filters on WFC3 (Trenti et al. 2011; Bradley et al. 2012; Trenti 2012; Schmidt et al. 2014; Bernard et al. 2016) explored 350 arcmin^2 and found 38 Y -band dropout candidates with $> L^*$, providing one of the strongest constraints on the $z \sim 8$ LF shape. The next iteration of the survey, BoRG [z9] (GO 13767, PI: M. Trenti), which we use in this study, is optimized for higher redshift ($z > 9$) galaxies with an updated set of five WFC3IR/UVIS filters (F300LP, F105W, F125W, F140W, and F160W). Preliminary results from this survey were presented in Calvi et al. (2016) and Morishita et al. (2018). We use the latest vetted sample of $z \sim 9$ and $z \sim 10$ from Morishita et al. (2018). They select $z \sim 9$ galaxies from F105W (Y band) dropouts and $z \sim 10$ from F125W (J band) dropouts. They combine the F140W (JH) and F160W (H band) filter images to generate a detection image in which the size is determined by Source Extractor (Bertin & Arnouts 1996; Holwerda 2005).

Source Extractor measures the half-light radii of objects through a simple growth curve approach: the pixels in an object stack are sorted, each pixel is reproduced 10 times and the point within which 50% of the flux is contained. This area (number of pixels) is then converted to a radius in arcseconds by $r_e = \text{platescale} \times \sqrt{A/2\pi}$.

Effective radii of high-redshift sources are typically determined with either GALFIT (Peng et al. 2010) or Source Extractor (Bertin & Arnouts 1996; Holwerda 2005). For drizzled images, like the CANDELS fields, GALFIT is the best option as it allows for different Sérsic profiles and a separate sky-subtraction. However, in the case of undithered Hubble imaging, the sampling of the image is not acceptable for the galfit hard limits. Because the GALFIT run parameters have to be fixed for small objects such as the ones studied here (e.g., fixed Sérsic parameter and axis ratio) and the proven robustness of Source Extractor effective radii, we use these here.

Huang et al. (2013) compare the performance of Source Extractor and GALFIT on artificial images at lower redshift and they find discrepancies in the effective radii of Source Extractor for the lower luminosity but more extended objects ($m = 26$, $r_e = 0''.48$ – $0''.75$) or brighter and more compact ($m = 24$, $r_e < 0''.05$) than those presented here. In the former case, Source Extractor overestimates effective radius and the in latter case, underestimates it. We caution that—once there is enough information for a profile fit—GALFIT will be less biased than Source Extractor but for the luminosity and size we are working with here, the difference will be minimal (see, e.g., Oesch et al. 2010). We convert these effective radii to kiloparsec by correcting for the point-spread function (PSF), $r_e(\text{cor}) = \sqrt{r_e^2 - 0.13^2}$ (the WFC3 PSF is $0''.13$ for H_{160}), and converting it to kiloparsec for the appropriate photometric redshift as determined in the H_{160} combined image by Morishita et al. (2018). Morishita et al. (2018) corrected their effective radii and luminosities already for the mild but significant lensing magnification they found in these galaxies by following the prescription by Mason et al. (2015b).

3. HST Colors and Sizes

Morishita et al. (2018) vetted their dropout galaxies through a combination of photo- z fits, visual inspection (including a size criterion), and complementary Spitzer observations when available. We use the complete list of candidate galaxies without the visual criterion of Morishita et al. (2018) applied.

A first check is to see if the HST colors and the effective radii of these candidate galaxies separate out the selected sources and the rejected sources. Morishita et al. (2018) present a color C1 and C2 in their tables. C1 is the $J_{125} - H_{160}$ or the $Y_{105} - JH_{140}$ for J - and Y -band dropouts, respectively $z \sim 9$ and $z \sim 10$ candidate galaxies. C2 is $JH_{140} - H_{160}$ for all objects.

Figure 1 shows colors and on-sky effective radii of the candidate sources and those selected by Morishita et al. (2018) as very probably $z \sim 9$ sources. Selection of the $z \sim 9$ galaxies is problematic to reproduce with a color- r_e selection based on HST colors. In Holwerda et al. (2015), it was shown that the $z \sim 9$ selection could be vetted with either effective radius or the H –[3.6] color and it was argued that effective radius could perhaps stand in for this color if not available. Figure 1 illustrates the problem with a single value size cut as a hard size criterion would effectively cull some interlopers but it would still leave a majority of contaminants. However, a declining probability of inclusion with size—which is implicitly done by

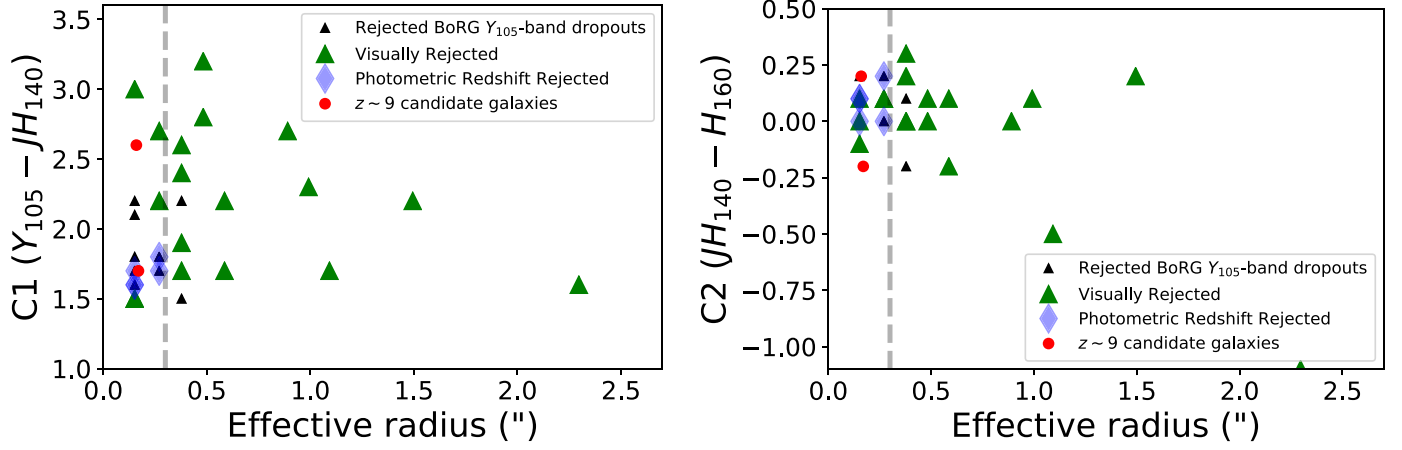


Figure 1. Effective radii vs. the two colors $Y_{105} - JH_{140}$ and $JH_{140} - H_{160}$ for the Y_{105} -band dropouts ($z \sim 9$ candidates). Green triangles and blue diamonds are candidates rejected visually and/or through their photo- z solution. Black triangles were rejected for a different reason, mostly their $H-3.6 \mu\text{m}$ color. The red points are the selected $z \sim 9$ candidate galaxies.

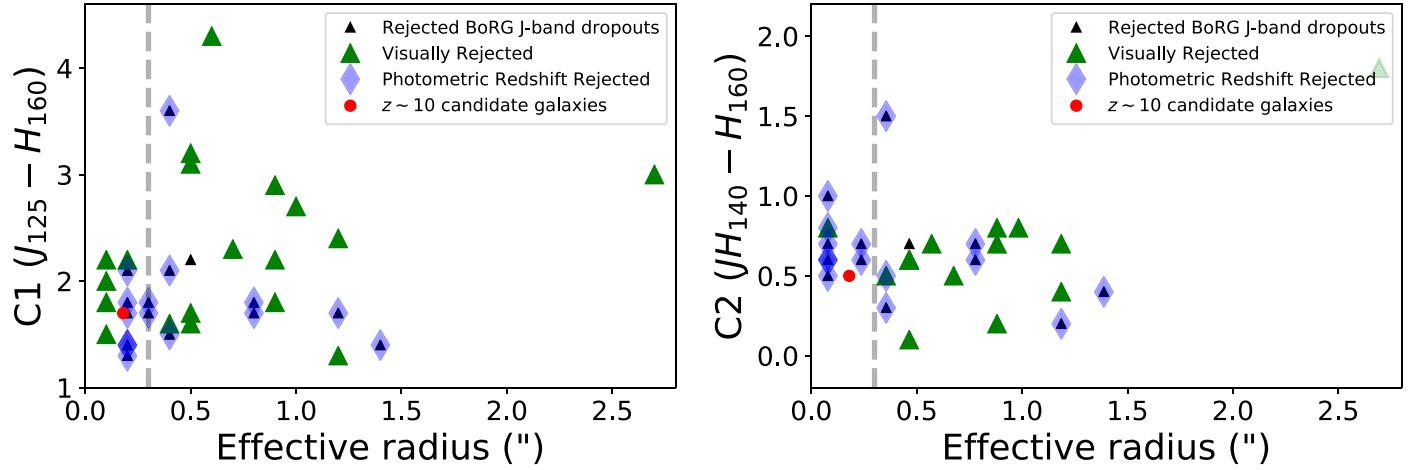


Figure 2. Effective radii vs. the two colors $J_{125} - H_{160}$ and $JH_{140} - H_{160}$ for the J_{125} -band dropouts ($z \sim 10$ candidates). Green and blue triangles are candidates rejected visually or through their photo- z solution. Black triangles were rejected for a different reason, mostly their $H-3.6 \mu\text{m}$. The red points are the selected $z \sim 10$ candidate galaxies.

visual inspection—could supplant the visual inspection in supplementing the photo- z rejections.

Figure 2 shows the two colors and the effective radii for the candidate objects and the single vetted $z \sim 10$ object. Here, the BoRG filter set does suggest a color-effective radius as a possible way to select highly likely $z \sim 10$ candidate galaxies. J -band dropouts are selected using a $J_{125} - H_{160} > 1.3$ and signal-to-noise ratio (S/N) constraints. In Figure 2 one could require $r_e < 0''.3$ and $JH_{140} - H_{160} < 0.55$ would cull most of interlopers that now were rejected visually, through their photometric redshift, or IRAC color. We argue here that the size may act as a prior to be included in photometric redshift selection. The strict effective radius criterion ($r_e < 0''.3$, where r_e is corrected for the PSF), results in a removal of 65%–70% of the visual rejections and $\sim 50\%$ of the all rejections in the $z = 9$ –10 samples.

A size criterion does select against the brightest galaxies in an LF due to the size–luminosity relation. At $z \sim 10$, an explicit criterion—rather than a more implicit visual one—of $0''.3$ translates to the 1.25 kpc limit and if earlier size–luminosity relations hold (e.g., Grazian et al. (2012) at $z \sim 7$) an effective cutoff at $M^* = 10^{10} M_\odot$ or $M_{UV} \sim -22.9$ or alternatively $M_{UV} \sim -28.2$ assuming the Holwerda et al. (2015) size–luminosity relation.

We argue that it is better to have this explicit bias with a cut in effective radius rather than an implicit size selection based on visual inspection. The absolute luminosity selected against however is predicted to be exceedingly rare at $z \sim 9$ –10 (see Bouwens et al. 2015; Finkelstein et al. 2015; Mason et al. 2015a).

One can compute the relative distribution of sizes of galaxies based on the simulated LF of Mason et al. (2015a), ranging from 3 mag brighter than M^* , $M = -24.5$ to $M = -10.5$, with an assumed size–luminosity relation, either the one from Grazian et al. (2012), for $z = 7$ galaxies or the one from Holwerda et al. (2015) for bright $z = 9$ –10 galaxies. There are uncertainties in the LF parameters from Mason et al. (2015a) as well as in the assumed luminosity–size relation. In addition, there is a measurement error in the effective radius which one can approximate with the WFC3 PSF width. Bootstrapping these into an uncertainty for the size function is illustrated in the Appendix.

Depending on the assumed size–luminosity relation, a size criterion for $z > 7$ galaxies of $0''.3$ (~ 1.25 kpc at $z = 9$) removes a small fraction of the total expected $z > 7$ population (see the Appendix and Figure 8). Figure 4 shows the total number of galaxies in the high-redshift universe as a function

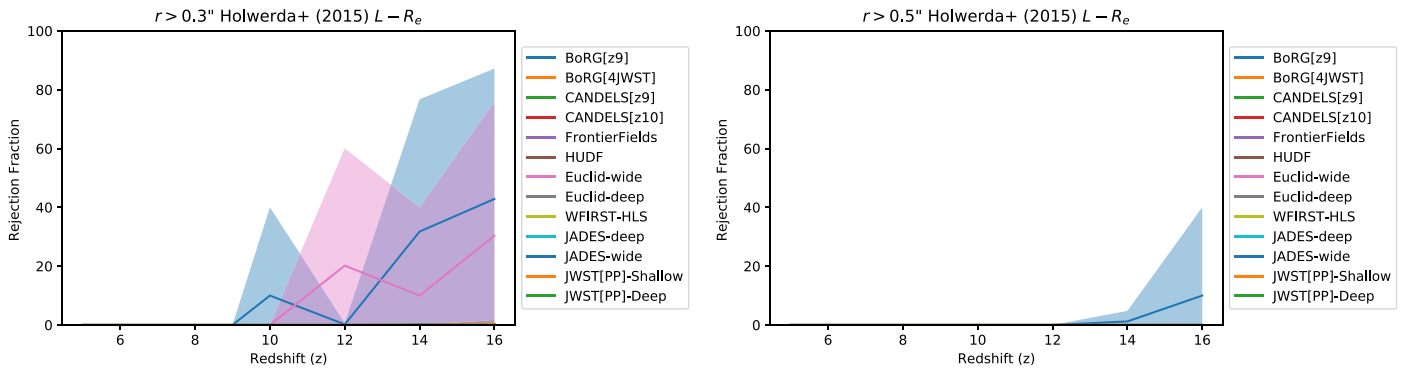


Figure 3. Rejection percentage of different surveys, assuming the Holwerda et al. (2015) luminosity–size relation and either a $r_e = 0''.3$ or $0''.5$ (right) selection criteria. BoRG[z9] rejection fractions reach 10% at $z = 10$ for $0''.3$.

of apparent size for $z = 7$ and $z = 9$ assuming either the Holwerda et al. (2015) or the Grazian et al. (2012) size–luminosity relation to show the spread in the size function. These examples illustrate the role the assumed size–luminosity relation plays in the loss estimate of an explicit size cut.

Given how uncertain the size–luminosity relation is at $z = 9 - 10$, any implicit (visual inspection) or explicit size criterion should be accounted for. Typical photometric contamination of high-redshift candidate galaxies is still $\sim 10\% - 50\%$ (see Figures 1 and 2). For comparison, the fraction of galaxies removed in a survey by a hard size cut depends strongly on the size–luminosity relation assumed and how far one is willing to extrapolate the LF by Mason et al. (2015a). If this is taken in extremis, one extends the LF so far there is no longer enough volume in the early universe to support a single galaxy of that size according to the LF (illustrated in Figure 4).

If one assumes just the luminosity range calculated in Mason et al. (2015a) as a viable range, the rejection rate is less than 1 ppm for either luminosity–size relation. If one limits oneself to 6 magnitudes brighter than the Mason et al. range and limit to the BoRG[z9] detection limit ($m_H = 23.6$; Rojas-Ruiz et al. 2020), one gets the rejection fraction of the total galaxy population tabulated in Table 1. Assuming the Holwerda et al. (2015) luminosity–size relation for bright sources at $z = 9$, the rejection rate by either size cut above $z = 5$ is much smaller compared to the contamination rate by interlopers from photometry alone within expected scatter (Table 1 and Figure 3). However, the loss rate is similar or worse to the contamination rate if one assumes the Grazian et al. (2012) luminosity–size relation for $z = 7$.

For candidates found in BoRG[z9], the luminosity–size relation for bright galaxies from Holwerda et al. (2015) is the most appropriate for $z = 9$ candidate objects. If one uses the $0''.3$ cut on BoRG[z9], this results in a mean rejection rate of 10% at $z = 10$ (Figure 3, Table 1). For comparison, close to half the candidate sources in Morishita et al. (2018) were rejected visually (Figures 1 and 2) making contamination from lower redshift sources a much greater concern.

We explored all other relevant discovery surveys (Euclid, Roman Space Telescope, James Webb Space Telescope (JWS), and HST CANDELS) to explore if other surveys would suffer similar rejection rates of bona fide high- z sources. Only Euclid would suffer from this with the strictest $0''.3$ size cut (assuming the luminosity–size relation from Holwerda et al. 2015), and only above $z = 10$ (Figure 3).

Table 1

The Loss Rate Percentage—the Percentage of All Detectable Galaxies at Each Redshift Removed—of the $0''.3$ and $0''.5$ Hard Cut Assuming One of the Two Different Size–Luminosity Relations and the Mason et al. (2015a) Luminosity Functions Over the Observable Luminosity Range for BoRG[z9]

z	Holwerda et al. (2015) (%)	Grazian et al. (2012) (%)
5.00	0.00 ± 0.00	15.26 ± 28.74
6.00	0.00 ± 0.02	25.86 ± 34.04
7.00	0.01 ± 0.07	47.27 ± 44.69
8.00	2.03 ± 14.00	72.10 ± 40.01
9.00	3.05 ± 17.06	88.40 ± 28.69
10.00	2.80 ± 15.96	95.85 ± 17.69
12.00	13.02 ± 32.85	99.96 ± 0.41
14.00	34.08 ± 47.32	99.76 ± 2.38
16.00	48.45 ± 48.38	100.00 ± 0.00
<hr/>		
5.00	0.00 ± 0.00	10.56 ± 22.82
6.00	0.00 ± 0.00	12.15 ± 24.88
7.00	0.00 ± 0.00	11.34 ± 24.82
8.00	0.00 ± 0.00	15.93 ± 27.75
9.00	0.00 ± 0.00	22.45 ± 34.60
10.00	0.00 ± 0.00	28.50 ± 38.84
12.00	0.00 ± 0.00	47.26 ± 45.16
14.00	2.00 ± 14.00	77.23 ± 37.32
16.00	3.03 ± 17.06	89.23 ± 29.67

Note. The error predominantly comes from uncertainty in the size–luminosity relation and the size measurement, assumed to be a WFC3/IR FWHM ($0''.1$).

Moving beyond hard cuts for high-redshift Lyman-break object selection, we would recommend a probabilistic approach with combined probability function over color, size, and perhaps including morphometrics (e.g., using asymmetry and Gini Kusmic et al. 2019) for candidate high-redshift source selection from source catalogs. In the lower redshift regime, photometric redshift estimates have included morphological information in addition to colors to improve reliability (e.g., Xia et al. 2009; Momcheva et al. 2016; Soo et al. 2018; Paul et al. 2018; Wilson et al. 2020).

Possible applications include GO^2LF , the Great Observatories Square-degree Legacy Fields (Stefanon et al. 2019), or future searches using HST, JWST, EUCLID, or Roman Space Telescope imaging, to include both morphometrics (Gini and asymmetry) as well as effective radius (e.g., a sharply declining prior above $0''.3$ and a $0''.5$ cutoff) for pre-selection of high-redshift candidate galaxies to substitute or prescreen before a visual inspection.

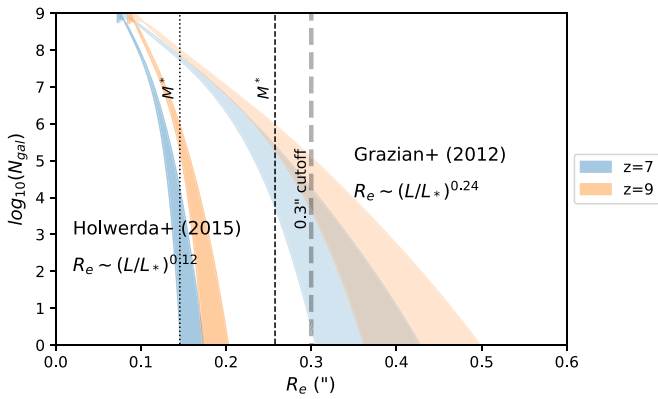


Figure 4. Total number of galaxies in the early universe as a function of observed effective radius, assuming the luminosity functions from Mason et al. (2015a) evaluated from $M = -38.5$ (~ 14 mag brighter than M^*) to $M = -10.5$, the two size–luminosity functions at higher redshift, (Grazian et al. 2012; Holwerda et al. 2015), and the volume available at each redshift. The width of the relation is an assumed error, the width of the WFC3 PSF ($0''.1$). The narrow lines are the point of M^* of the Mason et al. (2015a) luminosity function (dotted and dashed for the relative size–luminosity relations, respectively). The size cut of $0''.3$ would remove a very small fraction ($\ll 1$ ppm) of galaxies at $z \sim 9$ – 10 assuming the $z \sim 7$ size–luminosity relation from Grazian et al. (2012), a $0''.5$ hard size cut would remove none.

4. Effective Radius with Redshift

Morishita et al. (2018) computed the effective radius from the F160W (H_{160}) image, similar to most other studies on the size of high-redshift which use H_{160} (e.g., Holwerda et al. 2015; Shibuya et al. 2015). We therefore expect the Source Extractor sizes to align reasonably well with the GALFIT fit sizes (Peng et al. 2002, 2010) of previous studies. Morishita et al. (2018) corrected their luminosities and sizes already for the lensing magnification they determined affected the majority of their candidate $z \sim 9$ – 10 galaxies following the prescription in Mason et al. (2015a).

Figure 5 compares the effective radii from Morishita et al. (2018) to individual candidate galaxy sizes found by Holwerda et al. (2015), Bowler et al. (2017), Oesch et al. (2016), Salmon et al. (2018), and Bridge et al. (2019), and the mean values from Bouwens et al. (2004), Zheng et al. (2014), Oesch et al. (2010), Ono et al. (2013), and the mode values from Shibuya et al. (2015) for both star-forming galaxies (SFG) and Lyman-break galaxies (LBG). The best fit assuming $r_e \propto (1+z)^m$ from Holwerda et al. (2015) with $m = -1.32$ is also shown (thin dashed line), as is the nominal resolution of WFC3 (wide dashed gray line).

Shibuya et al. (2015) already pointed out that the distribution of galaxy sizes is not well characterized by a mean value but more accurately by a peak, characterized by the mode and a tail to higher values. Figure 6 shows the histogram of the effective radii of $z \sim 9$ – 10 candidate galaxies from Holwerda et al. (2015) and Morishita et al. (2018). The combined data set hints at the same peak and possibly a tail to higher values similar to the one Shibuya et al. (2015) identify at $z \sim 6$ redshifts where the statistics are better. The $z \sim 9$ show similar peak size as $z \sim 6$ but a lack of an extended wing thus far.

Low number statistics remain an issue and the current distribution of bright $z \sim 9$ galaxies is consistent with the distribution at $z \sim 6$. Curtis-Lake et al. (2016) point to a lack of size evolution $z > 4$ but as Shibuya et al. (2015) noted, this is more the effect of the choice between mean or mode used in characterizing the size evolution. The mode of the size

distribution evolves slowly with redshift and most of the more rapid evolution occurring in the tail of the size distribution, influencing the mean.

The gradual size evolution from $z \sim 9$ to lower redshifts appear in contrast to the potential strong evolution in the LF found by Bouwens et al. (2015) and Oesch et al. (2018). However, Morishita et al. (2018) already point out that their results on the brightest end of the LF ($L > 0.3L^*$) are completely consistent with both other BoRG results (Calvi et al. 2016) and other searches for high-redshift galaxies (Oesch et al. 2013, 2018; Bouwens et al. 2015; Bernard et al. 2016; Livermore et al. 2018) as well as theoretical predictions (e.g., Mason et al. 2015a). The majority of the strong evolution is happening at fainter luminosities than BoRG probes.

5. Star Formation Surface Density

Figure 7 shows the effective radius as a function of absolute magnitude in restframe ultraviolet with lines of constant star formation surface density marked following the relation in Ono et al. (2013). Neither dust extinction nor strong emission lines are assumed in this simple relation between size, absolute UV luminosity, and star formation surface density.

The $z \sim 9$ – 10 candidate galaxies from Holwerda et al. (2015) and Morishita et al. (2018) are similar in star formation surface density. Two exceptions are suggestive of much higher values ($\Sigma_{\text{SFR}} > 25M_{\odot} \text{ kpc}^{-2}$): 0956 + 2848-98 and 2229-0945-394. These higher star formation surface density candidate galaxies could be prime targets for spectroscopic follow-up with the aim to detect either the Ly α emission line or with the JWST for nebular emission lines.

Figure 7 compares the star formation surface densities found for the Holwerda et al. (2015) and Morishita et al. (2018) $z \sim 9$ objects to those found at lower redshift ($z \sim 7$; Bowler et al. 2017; Curtis-Lake et al. 2016; Grazian et al. 2017). The comparison to the Bowler et al. (2017) is instructive to show that the $z \sim 9$ sources are of comparable size and luminosity as the single $z \sim 7$ objects.

Kusmic et al. (2019) find that the morphometrics (asymmetry and Gini) of $z \sim 8$ candidate galaxies presented in Bridge et al. (2019) are consistent with mostly unperturbed galaxies in Lotz et al. (2010) and Curtis-Lake et al. (2016) but not with smooth Sérsic profiles. Our size–luminosity findings are consistent with no major mergers in this population: only very gradual evolution is needed to transition from these $z \sim 9$ sample of objects to the brighter, single $z \sim 7$ – 8 sources reported in Bowler et al. (2017) and Bridge et al. (2019).

We note here that higher redshift selection criteria, be it an explicit size criterion or a visual inspection, may select against potential ongoing mergers. Our size measurements are consistent with single objects only. This is not to be taken as evidence of an absence of galaxy mergers, just consistent with no mergers being selected at $z = 9$.

6. Concluding Remarks

We conclude that no clear HST color and effective radius cuts can really replace the visual inspection and photometric redshift check that Morishita et al. (2018) performed to vet all the initial candidates selected on dropout color for $z \sim 9$ (Y_{105} -dropouts) and $z \sim 10$ (J_{125} -dropouts). For the J_{125} -dropouts, a color–effective radius cut may be possible but the numbers are insufficient for a well motivated limit (Figure 2).

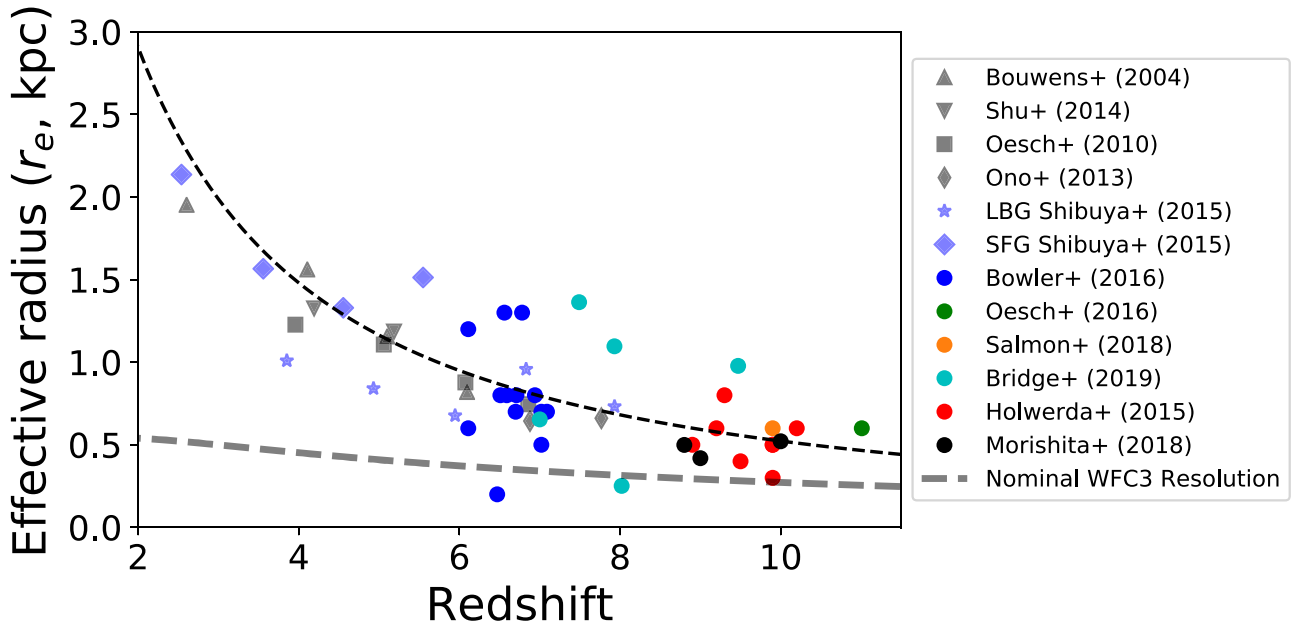


Figure 5. Relation between effective radius and redshift for the bright galaxies ($L > L_{z=3}^*$) from several previous studies: mean effective radii from Bouwens et al. (2004), Zheng et al. (2014), Oesch et al. (2010), and Ono et al. (2013; gray symbols), the mean values of the size distributions for the star-forming galaxies (SFG) and Lyman-break galaxies (LBG) from Shibuya et al. (2015) for comparison (light blue symbols), the effective radii as a function of redshift for individual galaxies from Holwerda et al. (2015; $z \sim 9$), Bowler et al. (2017), and Bridge et al. (2019; $z \sim 8$), and the $z \sim 9$ –10 galaxies identified by Morishita et al. (2018) that we discuss in the paper (circles). The dashed line is the best fit to $r_e \propto (1+z)^m$ from Holwerda et al. (2015) with $m = -1.32$, a value somewhere in between the two extreme cases. The mean values are for bright ($L > 0.3L^*$) galaxies while the mode is measured over the whole observed luminosity range but is dominated by lower luminosity ($L < 0.3L^*$) galaxies. The individual objects at the higher redshifts are predominantly bright and show a wide spread around the mean for bright sources.

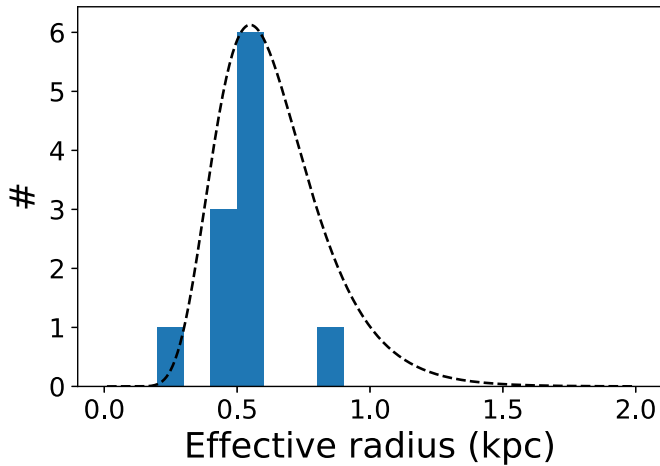


Figure 6. Histogram of the sizes of $z \sim 9$ –10 galaxies as identified by Holwerda et al. (2015) and Morishita et al. (2018) combined. The histogram follows a peak and tail to higher values of a log normal distribution that Shibuya et al. (2015) points out works well at lower redshifts ($z < 6$) for the size distribution of galaxies.

The selection with effective radius, rather than subjective one in a visual inspection may remove some of the ambiguity in selection however. An explicit size cut may remove the very brightest objects ($L \gg L^*$) in a survey, depending on the actual size–luminosity relation of the epoch. For example, the $0'3$ cut removes objects brighter than 2 mag than M^* at $z = 7$ –10 (Figure 8) but also 65%–70% of the visual rejections in the Morishita sample.

Rather than hard cuts in both color and effective radius, a probabilistic approach for Lyman break selection can be now considered. The prior for effective radius can drop off to zero between $0'3$ and $0'5$ for near-future HST-quality infrared data

set searches for high redshift, Lyman break candidates such as GO^2LF , JWST, targeted and parallel fields, Euclid, and Roman Space Telescope imaging.

The reported sizes from Morishita et al. (2018) are all consistent with $z = 9$ and $z = 10$ objects. The vetted sample from Morishita et al. (2018) appears to have successfully doubled the number of known bright candidate $z \sim 9$ –10 galaxies, ideal for future spectroscopic follow-up observations with, e.g., JWST and Keck.

The effective radii of the Morishita et al. (2018) $z \sim 9$ –10 galaxies are following the previously observed trend of the mean effective radius of high-redshift bright galaxies, following $r_e \propto (1+z)^{-1.3}$ (Figure 5). The distribution of all the $z \sim 9$ –10 galaxies also suggest strongly that the log normal distribution of bright galaxy sizes observed by Shibuya et al. (2015) holds out to this redshift (Figure 6).

The star formation surface densities implied by the size and luminosities of these $z \sim 9$ –10 galaxies is very comparable to those found in previous work on bright galaxies at these redshifts (Figure 7). In part this can be attributed to the selections by Morishita et al. (2018) against large galaxies. Size measurement of photometrically selected high-redshift galaxies remain a valuable and impartial a posteriori check of their high-redshift nature.

We thank the anonymous referee for the well thought-out, constructive, and thorough comments on earlier drafts. The effort and contributions are much appreciated.

This work was supported by a NASA Keck PI Data Award, administered by the NASA Exoplanet Science Institute. Data presented herein were obtained at the W. M. Keck Observatory from telescope time allocated to the National Aeronautics and Space Administration through the agency’s scientific partnership with the California Institute of Technology and the University of

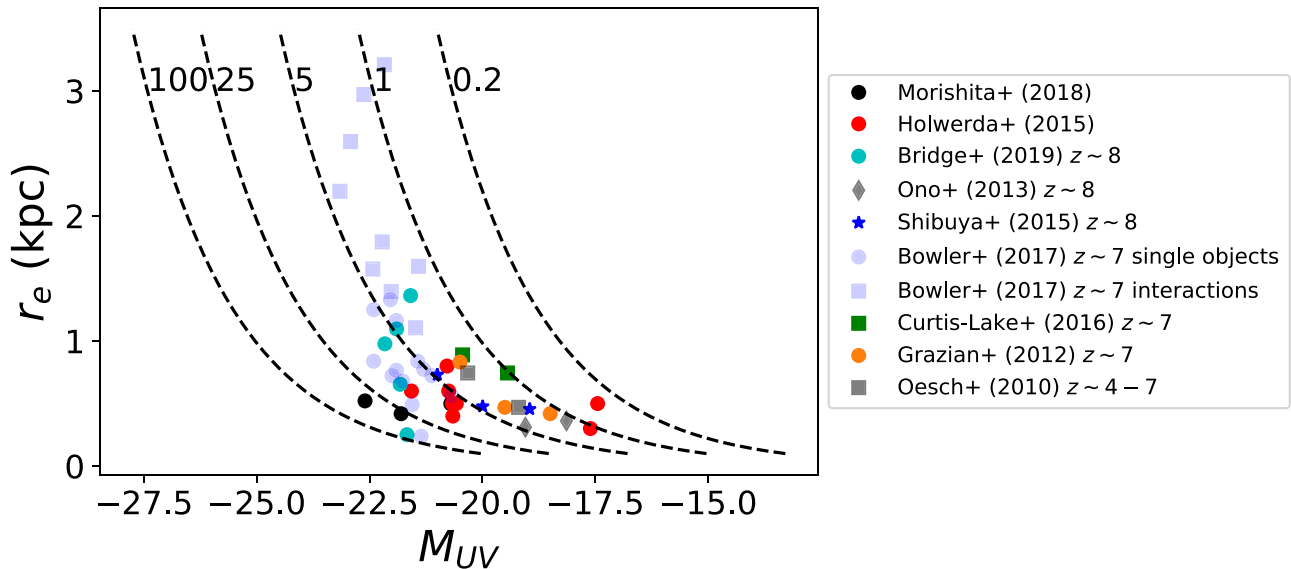


Figure 7. Absolute restframe ultraviolet magnitude vs. effective radius in kiloparsec for Holwerda et al. (2015) and Morishita et al. (2018) with lines of constant star formation surface densities ($\Sigma_{\text{SFR}}(M_{\odot} \text{ kpc}^{-2})$). The candidate galaxies from Morishita et al. (2018) appear to be at similar star formation densities to the sample found in Holwerda et al. (2015). For comparison, the $z \sim 7$ $r_e - M_{\text{UV}}$ relations from Bridge et al. (2019), Ono et al. (2013), Bowler et al. (2017), Curtis-Lake et al. (2016), Grazian et al. (2017), and Shibuya et al. (2015) are shown as well. Bowler et al. (2017) distinguishes between single objects and interactions. The Morishita et al. (2018) and Holwerda et al. (2015) $z \sim 9$ objects lie in the range for individual objects at $z \sim 7$.

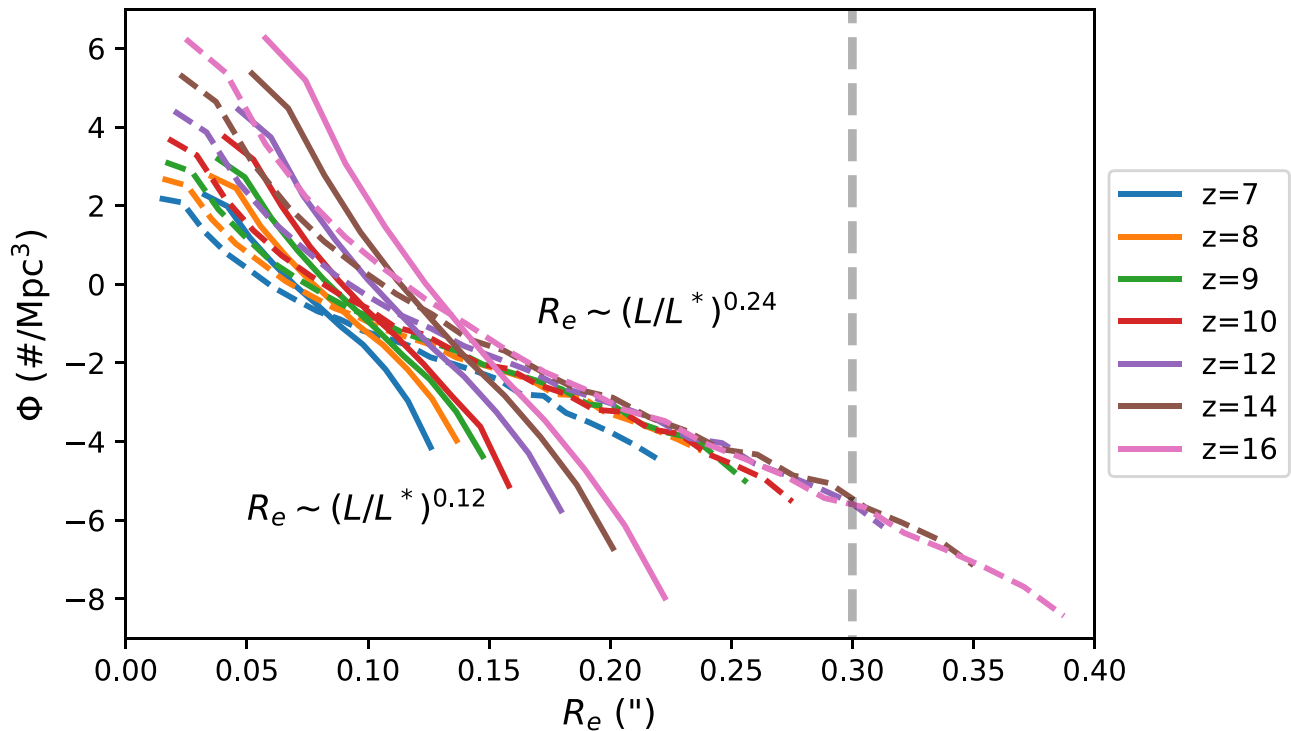


Figure 8. Distribution of observed effective radii, assuming the luminosity functions from Mason et al. (2015a) evaluated over $M = -22.5$ (~ 2 mag brighter than M^*) to $M = -10.5$ and two size–luminosity relations found at high redshift. The solid lines use the size–luminosity relation ($R \sim L/L^*$)^{0.12}, found for $z = 9 - 10$ galaxies in Holwerda et al. (2015) and the dashed lines the $z = 7$ size–luminosity relation ($R \sim L/L^*$)^{0.24}, presented in Grazian et al. (2012). Ono et al. (2013) found a much flatter distribution of sizes for high-redshift populations but thanks to the evolution in the luminosity function, >0.3 galaxies would still be very rare (Table 1).

California. The Observatory was made possible by the generous financial support of the W. M. Keck Foundation.

The authors wish to recognize and acknowledge the very significant cultural role and reverence that the summit of Maunakea has always had within the indigenous Hawaiian community. We are most fortunate to have the opportunity to conduct observations from this mountain.

This research has made use of the NASA/IPAC Extragalactic Database (NED) which is operated by the Jet Propulsion Laboratory, California Institute of Technology, under contract with the National Aeronautics and Space Administration. This research has made use of NASA’s Astrophysics Data System. This research made use of Astropy, a community-developed core Python package for Astronomy

(Astropy Collaboration et al. 2013). This research made use of matplotlib, a Python library for publication quality graphics (Hunter 2007). PyRAF is a product of the Space Telescope Science Institute, which is operated by AURA for NASA. This research made use of SciPy (Virtanen et al. 2020).

Appendix

Simulating the Loss Rate from a Hard Size Criteria

To estimate the loss rate from a hard size cut, we bootstrap the numbers of galaxies in the early universe using the Mason et al. (2015a) LF (their Table 1 and Figure 8). We evaluate two

size–luminosity relations, the one from Grazian et al. (2012) for $z = 7$ galaxies and the one from Holwerda et al. (2015) for the $z = 9$ population of galaxies to translate the evolution in the LF into a size distribution at different redshifts.

The uncertainties in the LF parameters (α , M^* , and $\log(\phi)$) are given in Mason et al. (2015a), their Table 1, the first two symmetric and the last one asymmetric. The uncertainties in the luminosity–size relations (normalization and exponent) are listed in Holwerda et al. (2015), Table 3, all assumed to be symmetric. We bootstrap the size distributions at each redshift in the Mason et al. (2015a) LFs 1000 times randomly varying

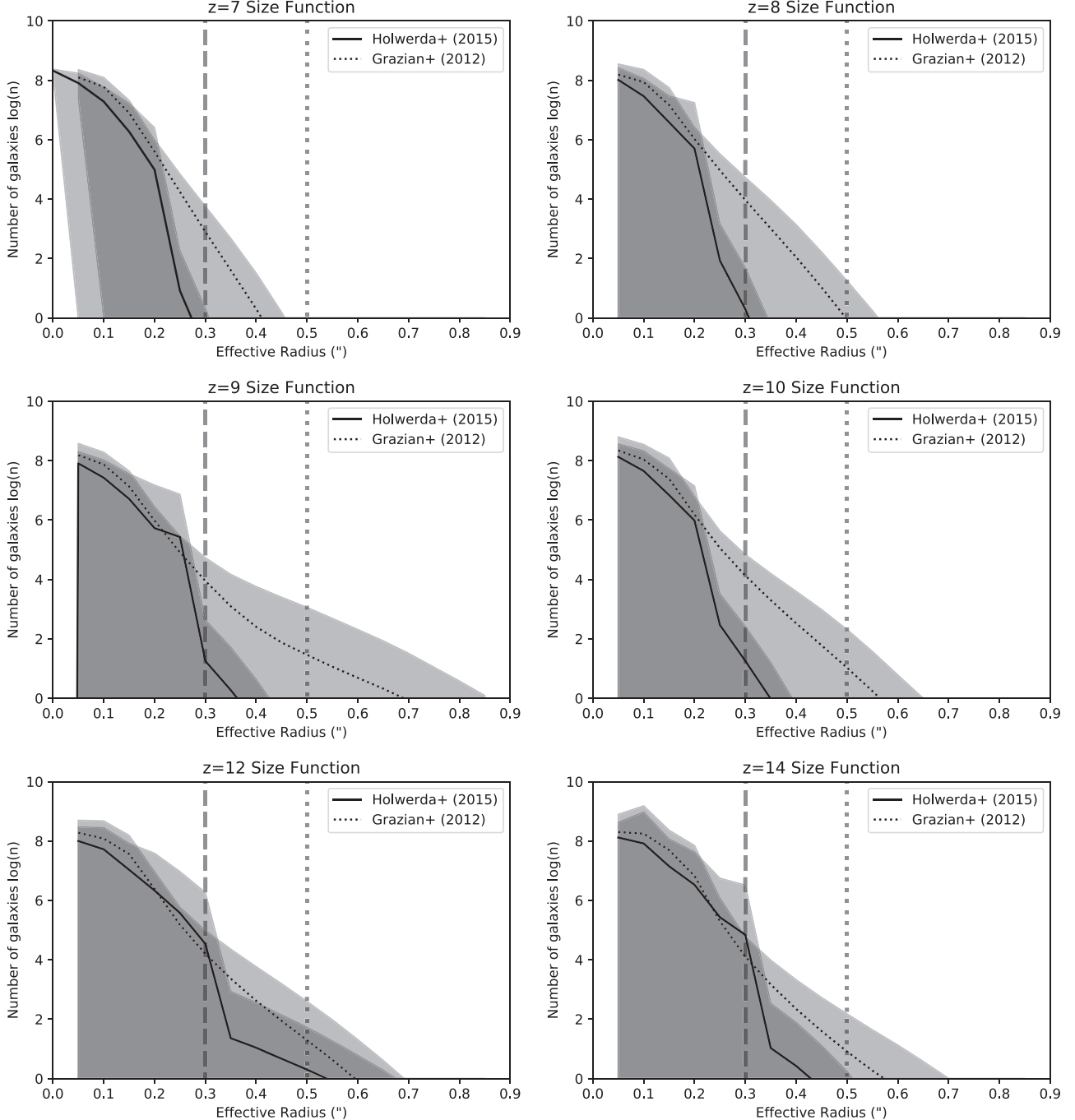


Figure A1. Mean and standard deviation variance of the size functions assuming the luminosity–size relation from either Grazian et al. (2012; dashed) or the Holwerda et al. (2015; solid) for the $z = 7$ –14 epochs. Uncertainty was bootstrapped using the Mason et al. (2015a) luminosity function uncertainties and those in each luminosity–size relation.

the LF and the luminosity–size relation according to their respective errors. The size distribution function is then subjected to a measurement error of $0''.1$. This is a fiducial error as many packages give no error (SOURCE EXTRACTOR), or a underestimated error based on a χ^2 value (e.g., GALFIT). It is the FWHM of the near-infrared instrumentation on HST and we assume it to be representative of the error in future observatories (Roman Space Telescope, Euclid, and JWST/NIRCam) at the same wavelengths.

Examples of the resulting size functions at $z = 7, 8,$ and 9 are in Figure A1. The evolution with redshift is noticeable but the difference in the assumed size–luminosity relation is driving the fraction of objects removed with a size cut. The mean and standard deviation of the fraction of galaxies rejected by a $0''.3$ or $0''.5$ size cut are listed in Table 1. We note that the uncertainty in the loss rate is much greater than the mean, principally because the uncertainties in the luminosity–size relations.

A hard size cut would not result in a significant loss of sample in the case of the Holwerda et al. (2015) relation but it could be as large as the contamination rate of bright sources if one assumes the Grazian et al. (2012) relation. And since these loss rates are for individual sources, close pairs or mergers might be excluded altogether, which is also an issue for visual inspection. With that in mind, using size as a Bayesian prior for high-redshift candidacy (flat to $0''.3$ and dropping zero at $0''.5$).

ORCID iDs

Benne W. Holwerda  <https://orcid.org/0000-0002-4884-6756>

Joanna S. Bridge  <https://orcid.org/0000-0002-8584-1903>

Rebecca L. Steele  <https://orcid.org/0000-0001-9537-5814>

Samir Kusmic  <https://orcid.org/0000-0002-0761-1985>

Larry Bradley  <https://orcid.org/0000-0002-7908-9284>

Rachael Livermore  <https://orcid.org/0000-0003-4456-1566>

Stephanie Bernard  <https://orcid.org/0000-0003-0956-0728>

References

- Astropy Collaboration, Robitaille, T. P., Tollerud, E. J., et al. 2013, *A&A*, **558**, A33
- Barone-Nugent, R. L., Trenti, M., Wyithe, J. S. B., et al. 2014, *ApJ*, **793**, 17
- Bernard, S. R., Carrasco, D., Trenti, M., et al. 2016, *ApJ*, **827**, 76
- Bertin, E., & Armouts, S. 1996, *A&AS*, **117**, 393
- Bouwens, R. J., Illingworth, G. D., Blakeslee, J. P., Broadhurst, T. J., & Franx, M. 2004, *ApJL*, **611**, L1
- Bouwens, R. J., Illingworth, G. D., Blakeslee, J. P., & Franx, M. 2006, *ApJ*, **653**, 53
- Bouwens, R. J., Illingworth, G. D., Labbe, I., et al. 2011a, *Natur*, **469**, 504
- Bouwens, R. J., Illingworth, G. D., Oesch, P. A., et al. 2011b, *ApJ*, **737**, 90
- Bouwens, R. J., Illingworth, G. D., Oesch, P. A., et al. 2015, *ApJ*, **803**, 34
- Bouwens, R. J., Oesch, P. A., Illingworth, G. D., et al. 2013, *ApJL*, **765**, L16
- Bowler, R. A. A., Dunlop, J. S., McLure, R. J., et al. 2015, *MNRAS*, **452**, 1817
- Bowler, R. A. A., Dunlop, J. S., McLure, R. J., & McLeod, D. J. 2017, *MNRAS*, **466**, 3612
- Bradley, L. D., Trenti, M., Oesch, P. A., et al. 2012, *ApJ*, **760**, 108
- Bridge, J. S., Holwerda, B. W., Stefanon, M., et al. 2019, *ApJ*, **882**, 42
- Calvi, V., Trenti, M., Stiavelli, M., et al. 2016, *ApJ*, **817**, 120
- Coe, D., Zitrin, A., Carrasco, M., et al. 2013, *ApJ*, **762**, 32
- Curtis-Lake, E., McLure, R. J., Dunlop, J. S., et al. 2016, *MNRAS*, **457**, 440
- Ellis, R. S., McLure, R. J., Dunlop, J. S., et al. 2013, *ApJL*, **763**, L7
- Fall, S. M., & Efstathiou, G. 1980, *MNRAS*, **193**, 189
- Ferguson, H. C., Dickinson, M., Giavalisco, M., et al. 2004, *ApJL*, **600**, L107
- Finkelstein, S. L., Song, M., Behroozi, P., et al. 2015, *ApJ*, **814**, 95
- Grazian, A., Castellano, M., Fontana, A., et al. 2012, *A&A*, **547**, A51
- Grazian, A., Giallongo, E., Paris, D., et al. 2017, *A&A*, **602**, A18
- Grogin, N. A., Kocevski, D. D., Faber, S. M., et al. 2011, *ApJS*, **197**, 35
- Hathi, N. P., Jansen, R. A., Windhorst, R. A., et al. 2008, *AJ*, **135**, 156
- Holwerda, B. W. 2005, arXiv:astro-ph/0512139
- Holwerda, B. W., Baldry, I. K., Alpaslan, M., et al. 2015, *MNRAS*, **449**, 4277
- Huang, K.-H., Ferguson, H. C., Ravindranath, S., & Su, J. 2013, *ApJ*, **765**, 68
- Hunter, J. D. 2007, *CSE*, **9**, 90
- Ishigaki, M., Kawamata, R., Ouchi, M., et al. 2018, *ApJ*, **854**, 73
- Koekemoer, A. M., Faber, S. M., Ferguson, H. C., et al. 2011, *ApJS*, **197**, 36
- Kusmic, S., Holwerda, B. W., Bridge, J. S., & Steele, R. L. 2019, *RNAAS*, **3**, 134
- Larson, R. L., Finkelstein, S. L., Pirzkal, N., et al. 2018, *ApJ*, **858**, 94
- Livermore, R. C., Trenti, M., Bradley, L. D., et al. 2018, *ApJL*, **861**, L17
- Lotz, J. M., Jonsson, P., Cox, T. J., & Primack, J. R. 2010, *MNRAS*, **404**, 590
- Madau, P., & Dickinson, M. 2014, *ARA&A*, **52**, 415
- Mason, C. A., Trenti, M., & Treu, T. 2015a, *ApJ*, **813**, 21
- Mason, C. A., Treu, T., Schmidt, K. B., et al. 2015b, *ApJ*, **805**, 79
- McCracken, H. J., Milvang-Jensen, B., Dunlop, J., et al. 2012, *A&A*, **544**, A156
- Mo, H. J., Mao, S., & White, S. D. M. 1998, *MNRAS*, **295**, 319
- Momcheva, I. G., Brammer, G. B., van Dokkum, P. G., et al. 2016, *ApJS*, **225**, 27
- Morishita, T., Trenti, M., Stiavelli, M., et al. 2018, *ApJ*, **867**, 150
- Oesch, P. A., Bouwens, R. J., Illingworth, G. D., et al. 2010, *ApJL*, **709**, L16
- Oesch, P. A., Bouwens, R. J., Illingworth, G. D., et al. 2013, *ApJ*, **773**, 75
- Oesch, P. A., Bouwens, R. J., Illingworth, G. D., et al. 2014, *ApJ*, **786**, 108
- Oesch, P. A., Bouwens, R. J., Illingworth, G. D., Labbé, I., & Stefanon, M. 2018, *ApJ*, **855**, 105
- Oesch, P. A., Brammer, G., van Dokkum, P. G., et al. 2016, *ApJ*, **819**, 129
- Oesch, P. A., van Dokkum, P. G., Illingworth, G. D., et al. 2015, *ApJL*, **804**, L30
- Ono, Y., Ouchi, M., Curtis-Lake, E., et al. 2013, *ApJ*, **777**, 155
- Paul, N., Virag, N., & Shamir, L. 2018, *Galax*, **6**, 64
- Peng, C. Y., Ho, L. C., Impey, C. D., & Rix, H. 2002, *AJ*, **124**, 266
- Peng, C. Y., Ho, L. C., Impey, C. D., & Rix, H. 2010, *AJ*, **139**, 2097
- Roberts-Borsani, G. W., Bouwens, R. J., Oesch, P. A., et al. 2016, *ApJ*, **823**, 143
- Rojas-Ruiz, S., Finkelstein, S. L., Bagley, M. B., et al. 2020, *ApJ*, **891**, 146
- Salmon, B., Coe, D., Bradley, L., et al. 2018, *ApJL*, **864**, L22
- Schmidt, K. B., Treu, T., Trenti, M., et al. 2014, *ApJ*, **786**, 57
- Shibuya, T., Ouchi, M., & Harikane, Y. 2015, *ApJS*, **219**, 15
- Soo, J. Y. H., Moraes, B., Joachimi, B., et al. 2018, *MNRAS*, **475**, 3613
- Stark, D. P., Ellis, R. S., Charlot, S., et al. 2017, *MNRAS*, **464**, 469
- Stefanon, M., Bouwens, R. J., Labbé, I., et al. 2017, *ApJ*, **843**, 36
- Stefanon, M., Brammer, G., Bouwens, R., et al. 2019, GO²LFG: Great Observatories Square-degree Legacy Fields, Spitzer Proposal **14253**
- Steidel, C. C., Adelberger, K. L., Giavalisco, M., Dickinson, M., & Pettini, M. 1999, *ApJ*, **519**, 1
- Trenti, M. 2012, in AIP Conf. Ser. 1480, First Stars IV: from Hayashi to the Future, ed. M. Umemura & K. Omukai (Melville, NY: AIP), **238**
- Trenti, M., Bradley, L. D., Stiavelli, M., et al. 2011, *ApJL*, **727**, L39
- Trenti, M., Bradley, L. D., Stiavelli, M., et al. 2012, *ApJ*, **746**, 55
- Trenti, M., & Stiavelli, M. 2008, *ApJ*, **676**, 767
- Virtanen, P., Gommers, R., Oliphant, T. E., et al. 2020, *NatMe*, **17**, 261
- Wilson, D., Nayyeri, H., Cooray, A., & Häußler, B. 2020, *ApJ*, **888**, 83
- Xia, L., Cohen, S., Malhotra, S., et al. 2009, *AJ*, **138**, 95
- Zheng, W., Postman, M., Zitrin, A., et al. 2012, *Natur*, **489**, 406
- Zheng, W., Shu, X., Moustakas, J., et al. 2014, *ApJ*, **795**, 93
- Zitrin, A., Labbé, I., Belli, S., et al. 2015, *ApJL*, **810**, L12